Pressure Buffering Control to Reduce Pollution and Improve Flow Stability in Industrial Gas Headers

A.J. Wiid[a], J.D. le Roux[a], I.K. Craig[a,*]

[a]*Department of Electrical, Electronic, and Computer Engineering, University of Pretoria, Pretoria, South Africa.*

Abstract

This paper describes various regulatory and advanced control schemes which can be applied to industrial gas headers. The intention is to exploit the buffering capacity for pollution control as well as improve flow stability for consumers. The control schemes are compared using a Monte Carlo simulation on a simulated case study and a sensitivity analysis is done to evaluate the impact of variations in the gas properties on the cost functions. A compensated linear model predictive controller (CLMPC) is implemented on a real industrial header and compared with standard proportional-integral (PI) control. It is found that gas emissions and consumer stability can be substantially improved by intelligently utilising the available pressure buffering capacity in industrial gas headers.

Keywords: averaging control; control applications; gas emissions; gas pipelines; model predictive control; pollution control; pressure control; PID

1. Introduction

Industrial gas headers are used to transport gas between processing units in gas-to-liquid (GTL), and coal-to-liquid (CTL) factories. These streams in the gas phase include: synthetic gas (Syngas) obtained from the gasification of coal or the reforming of natural gas, tail gas and methane-rich gas as by-products from the Fischer–Tropsch process, industrial fuel gas systems, and utilities such as steam and oxygen. An example of a typical integrated CTL and GTL facility is shown in Fig. 1 indicating the locations of the various gas headers [1, 2, 3, 4, 5].

These headers normally use flaring or venting for pressure control in order to protect the downstream and upstream processing units from flow upsets. Header disturbances can originate from a variety of sources such as batch processes, upstream or downstream load changes, and process upsets. Flaring and venting wastes valuable feedstock, causes expensive economic penalties, releases greenhouse gasses, and negatively contributes to the processing carbon footprint [6, 7, 8, 9, 10].

Increasing environmental concerns have imposed tighter constraints on the economic operation of these these CTL and GTL production facilities [8, 9, 11, 12]. Therefore, although flaring and venting were incorporated into processes in the design phase with the intent of pressure control and stability, such actions are becoming increasingly problematic as a result of financial concerns and pressure resulting from Environmental, Social and Governance (ESC) investment practices [13].

The inherent problem to solve is the trade-off between process stability and gas release in the form of flaring or venting.

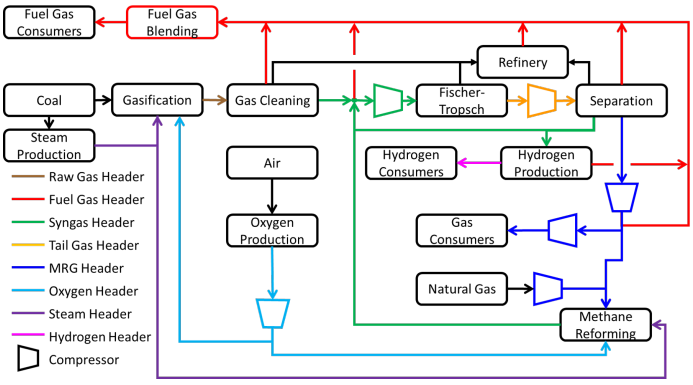

Figure 1: Integrated CTL and GTL facility with supporting fuel gas, steam, and oxygen utilities.

It has become crucial to not only ensure stability for consumers and suppliers, but also to minimise energy consumption and to minimise flaring and venting in gas headers. The objective of this work is to show that flaring and venting from industrial gas headers can be mitigated by utilising the inherent storage capacity of the gas header inventories similar to [14, 15, 16] for natural gas network energy optimisation. Additionally, gas network operations can be economically optimised through the intelligent use of available manipulated variables [17, 18]. These objectives can be realised through the design and implementation of suitable control strategies.

The multivariate nature of the gas headers, the fast dynamics and the tight header pressure constraints makes model predictive control (MPC) a suitable and attractive solution. Various types of MPC strategies have been developed for gas headers and networks [17, 18]. A difference between most of the MPC strategies previously developed and those developed in

*Corresponding author. Address: Department of Electrical, Electronic, and Computer Engineering, University of Pretoria, Pretoria, South Africa.
Tel.: +27 12 420 2172; fax: +27 12 362 5000.
Email address: ian.craig@up.ac.za (I.K. Craig)

this study, is that previous studies mostly consider larger and longer pipelines spanning between fifty to hundreds of kilometres as opposed the headers in this study spanning hundreds of meters to a few kilometres. Therefore, the dynamics of industrial headers in CTL and GTL factories are comparatively faster and has significantly less buffering capacity volume as opposed to the larger gas pipelines used to transport gasses over large distances. Although the simulation framework and industrial case study are representative of typical headers found in CTL and GTL factories, the solutions can potentially be applied to a wider range of gas header and pressure control applications.

The problem of designing a control scheme to make use of the available buffer capacity (the difference between the level set-point (SP) and the maximum and minimum values) to improve flow stability has been widely studied for liquids and is known as averaging level control. Examples include proportional-integral-derivative (PID) controller tuning rules [19, 20, 21, 22, 23, 24], piecewise-linear control [20, 25, 26], range control [19], non-linear control [20, 22, 26, 27, 28, 29, 30], optimal control [24, 29, 31, 32, 33], and MPC [19, 30, 34, 35, 36]. Some of the proposed control schemes for averaging level control are adapted in this work for pressure buffering applications and compared using chosen metrics.

Level averaging control differs from pressure buffering control due to the following considerations:

- Header pressure control is non-linear when compared to level control due to the effects of temperature, composition, and the compressibility of gasses.
- In general, there is less buffering capacity in gas headers than liquid storage drums due to the design intent.
- In general, the impact of upsets are more pronounced in gas processing units. The gas units are more interconnected than liquid processing units due to the interdependence of upstream and downstream units on the pressure profile. In contrast, liquid processing units are generally segregated by storage drums and buffering tanks.
- Averaging level control is only dependant on the mass balance where pressure headers are governed by the mass and momentum balances as well as the equations of state.
- The pressure response in gas headers may include large process phase lags or inverse responses depending on the measuring location on the pipe [37]. Liquid storage drums typically do not exhibit large phase lags and only have inverse responses in specialised processes such as boiler steam drums.

Therefore, the control schemes proposed for level averaging control cannot be directly applied to the pressure headers without further investigation.

Various control schemes are presented in this work for pressure buffering control in industrial gas headers. The purpose of comparing these schemes is not to select a *best* performing controller but rather to provide an overview of the various options available. The aim of this paper is to cultivate awareness of the buffering capacity available within gas headers and the various control schemes available to exploit this capacity for improved consumer stability and pollution control. A selection can then be made based on software functionality available, solution complexity, ease of implementation and maintenance, and desired performance. Additionally, it is beneficial in practice to design a suitable fall-back strategy in the redundant regulatory control layer when the advanced schemes are turned off.

The paper is organised as follows. Section 3 describes the non-linear state-space model used in the simulations and MPC applications. Section 2 introduces the simulation case-study process and model parameters used in this study. Section 4 illustrates various buffering pressure control schemes. Specifically, Section 4.1 briefly explains regulatory pressure-flow cascade strategies used in the gas header pressure control schemes in this study, Section 4.2 discusses various regulatory and advanced regulatory schemes applied to gas headers for pressure buffering control, and Section 4.4 expands on MPC applications which can be applied to gas headers. Section 5 compares the various control schemes in simulation when applied to the case study introduced in Section 2 using a Monte Carlo simulation. Furthermore, a sensitivity study is conducted on the individual influence of the gas properties on the cost functions used as metrics in the Monte Carlo simulation. Section 6 presents a real world implementation of a pressure buffering control scheme on an industrial gas header. Section 7 concludes the study.

2. Simulation Model Description

The process shown in Fig. 2 is an example of a typical process and used as the simulation case study in this work. Other configurations are possible. P_z and Q_z are the header inlet pressure and flow rate, and P_L and Q_L are the header outlet pressure and flow rate respectively. The process feed (Q_D) is supplied to the header inlet and cannot be manipulated. Gas can be flared at the inlet of the header (Q_F) during high pressure scenarios and pulled in from an expensive supplier (Q_S) during low pressure scenarios. The header outlet supplies gas to one consumer (Q_V) which can be manipulated. The dashed red lines in Fig. 2 indicate manipulated flow rates.

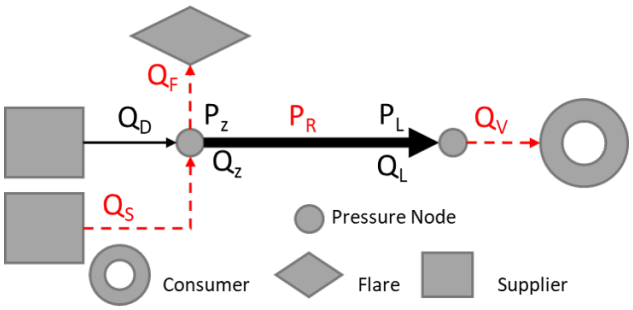

Figure 2: Simulation case study process diagram. The dashed red lines indicate manipulated flow rates.

The gas pressure measures the imbalance between gas generation and consumption. Since consumers define the gas flow

rate they require, a change in the sum of flows required may produce an imbalance between gas generation and consumption which necessitates flaring. The pipe pressures have high and low constraints and do not have to be controlled tightly at SP. It is desirable to minimise flaring and provide stability for the consumer flow rates by absorbing load changes from the supplier. Load changes in the gas flow rate result in self-regulatory responses and off-sets in the mass balance result in integrating responses [37, 38]. Since the pressure control is dependent on the mass balance, it has an integrating response.

It should be noted that the following steady state mass balances hold for the pressure nodes in Fig. 2:

$$Q_z = Q_D - Q_F + Q_S, \tag{1a}$$
$$Q_L = Q_V. \tag{1b}$$

The cost of flaring (2a), consumer stability (2b), and expensive supplier use (2c) is expressed as,

$$J_F = \frac{\sum_{k=1}^{S} Q_{F,t_k}}{S\ W_1}, \tag{2a}$$
$$J_V = \frac{1}{S\ W_2} \sum_{k=1}^{S} \left| \frac{Q_{V,t_k} - Q_{V,t_{k-1}}}{t_k - t_{k-1}} \right|, \tag{2b}$$
$$J_S = \frac{\sum_{k=1}^{S} Q_{S,t_k}}{S\ W_3}. \tag{2c}$$

S is the total amount of time steps used to normalise the cost function to the simulation time interval, k is the current time step, and the weights W_1, W_2, and W_3 are used to scale the values relative to their economic penalty. W_1 is directly used to penalise emissions which contributes to pollution and wastes feedstock, W_2 is used to penalise large movements in the consumer flow rate, and W_3 is used to penalise utilising the expensive supplier for pressure control. The total cost is calculated as,

$$J_T = J_F + J_V + J_S. \tag{3}$$

The chosen pressure measurement P_R, used as the controlled variable, may be located anywhere on the header [37]. P_R is not allowed to violate the low pressure limit ($\underline{P}_R$) and high pressure limit ($\bar{P}_R$). The pressure constraints are usually determined by design and process constraints. Additionally, there may exist dynamic upper ($\bar{Q}$) and lower ($\underline{Q}$) limitations on the individual flow variables. The flow constraints may be due to design constraints, or move based on upstream and downstream process requirements. The pressure and flow constraints are shown as,

$$\underline{P}_R \le P_R(t) \le \bar{P}_R \quad \forall \quad t \ge 0, \tag{4a}$$
$$\underline{Q}_S(t) \le Q_S(t) \le \bar{Q}_S(t) \quad \forall \quad t \ge 0, \tag{4b}$$
$$\underline{Q}_V(t) \le Q_V(t) \le \bar{Q}_V(t) \quad \forall \quad t \ge 0, \tag{4c}$$
$$\underline{Q}_F(t) \le Q_F(t) \le \bar{Q}_F(t) \quad \forall \quad t \ge 0. \tag{4d}$$

Table 1 provides the nominal simulation parameters used in the simulation environment.

Table 1: Simulation case study model parameters.

Parameter	Value	Units
Inlet Pressure (P_z)	3x10^3	kPa
Outlet Pressure (P_L)	$P_z - \frac{fZR\ TQ\|Q\|L}{2DA^2M_wP_z}$	kPa
Mass Flow (Q)	10	kg/s
Friction (f)	0.02	-
Compressibility (Z)	0.95	-
Gas Constant (R)	8314	J/kgK
Temperature (T)	300	K
Molecular Weight (M_w)	17.2	kg/kmol
Pipe length (L)	5000	m
Pipe Diameter (D)	0.38	m
Pipe Segments (n)	2	-
Polynomial Order (N)	3	-
Time Step Size (Δt)	1	s

3. State-Space Model

This section provides a brief summary of the state-space model used this study. The model nomenclature is shown in Table 1. A more detailed model description can be found in [37, 38].

Pressure headers can be suitably described by the governing equations,

$$\frac{\partial P}{\partial t} + \frac{ZR\,T}{AM_w}\frac{\partial Q}{\partial z} = 0, \tag{5a}$$
$$\frac{\partial Q}{\partial t} + A\frac{\partial P}{\partial z} + \frac{fZR\,TQ|Q|}{2DAM_wP} = 0, \tag{5b}$$
$$PAL - \frac{mZRT}{M_w} = 0, \tag{5c}$$

where the momentum and continuity equations are shown by (5a) and (5b) respectively [18, 38]. P is the pressure, Q is the mass flow rate, R is the gas constant, A is the cross sectional area of the pipe, L is the full pipe length, Z is the gas compressibility, T is the temperature, f is the coefficient of friction, D the pipe diameter, m is the gas mass, and M_w is the mixed gas molecular weight. t is time and z is length taken in the same direction as the pipe length L. The gas properties are related to each other within the pipe with an equation of state (5c), in particular, the ideal gas law compensated for compressibility is used.

Applying the spectral element method to spatially discretise the system [38], the final global system of equations are,

$$\frac{d\boldsymbol{P}}{dt} = M_\kappa^{-1}[S\,\boldsymbol{Q} + Q_z\boldsymbol{b_0} - Q_L\boldsymbol{b_L}], \tag{6a}$$
$$\frac{d\boldsymbol{Q}}{dt} = M_\alpha^{-1}[S\,\boldsymbol{P} - M_\tau\boldsymbol{\Theta} + P_z\boldsymbol{b_0} - P_L\boldsymbol{b_L}], \tag{6b}$$

where $M_{\kappa,\alpha,\tau}$ are the mass matrices and S is the stiffness matrix

and (6) is condensed as,

$$\dot{\boldsymbol{x}} = \boldsymbol{f}(\boldsymbol{x}, \boldsymbol{u}) = \left[\frac{d\boldsymbol{P}^T}{dt}, \frac{d\boldsymbol{Q}^T}{dt} \right]^T. \tag{7}$$

The vectors indicated in bold are defined as,

$$\boldsymbol{P} = [P_1, \ldots, P_c]^T, \tag{8a}$$
$$\boldsymbol{Q} = [\tilde{Q}_1, \ldots, \tilde{Q}_c]^T, \tag{8b}$$
$$\boldsymbol{\Theta} = \left[\frac{\tilde{Q}_1|\tilde{Q}_1|}{P_1}, \ldots, \frac{\tilde{Q}_c|\tilde{Q}_c|}{P_c} \right]^T. \tag{8c}$$

c is equal to the total number of collocation points calculated as $nN+1$ and is dependant on the number of pipe segments (n) and polynomial order (N) used to spatially discretise the governing equations. The boundary vectors are of the same length as (8) and are defined as,

$$\boldsymbol{b_0} = [1, 0, \ldots, 0]^T, \tag{9a}$$
$$\boldsymbol{b_L} = [0, \ldots, 0, 1]^T. \tag{9b}$$

The boundary conditions Q_z, Q_L, P_z, and P_L for a pipe of length L are defined as,

$$Q_z = Q(0, t) \quad \text{and} \quad Q_L = Q(L, t), \tag{10a}$$
$$P_z = P(0, t) \quad \text{and} \quad P_L = P(L, t). \tag{10b}$$

The pipe inlet (Q_z) and outlet (Q_L) flows are chosen as model inputs,

$$\boldsymbol{u} = [Q_z, Q_L]^T. \tag{11}$$

The boundary pressures are given by the following substitutions,

$$P_z = P_1 - \sqrt{\frac{ZR\,T}{M_w}} \frac{AM_w}{2ZR\,T} (\tilde{Q}_1 - u_1), \tag{12a}$$
$$P_L = P_c - \sqrt{\frac{ZR\,T}{M_w}} \frac{AM_w}{2ZR\,T} (u_2 - \tilde{Q}_c). \tag{12b}$$

The model outputs are any pipe pressures at the collocation points extracted as values from the vector $\boldsymbol{P}$,

$$\boldsymbol{y} = \boldsymbol{g}(\boldsymbol{x}, \boldsymbol{u}) = C\boldsymbol{P}. \tag{13}$$

where the matrix C is chosen to extract the desired pressures at the collocation points. The outputs are used as measured states for the simulated process in this study.

The final state-space model of the system is as follows,

$$\dot{\boldsymbol{x}} = \boldsymbol{f}(\boldsymbol{x}, \boldsymbol{u}) + \boldsymbol{d}_{P,Q}, \tag{14a}$$
$$\boldsymbol{y} = \boldsymbol{g}(\boldsymbol{x}, \boldsymbol{u}) + \boldsymbol{v}. \tag{14b}$$

Measurement noise is simulated by adding noise to the measured output pressures $\boldsymbol{v} \sim \mathcal{N}(0, \sigma_v^2)$, and process noise to the plant pressure states $\boldsymbol{d}_P \sim \mathcal{N}(0, \sigma_{d_P}^2)$, and flow states $\boldsymbol{d}_Q \sim \mathcal{N}(0,\ \sigma_{d_Q}^2)$ respectively. Noise is used when the model is used to simulate the process and is excluded when the model is used in model predictive applications.

4. Pressure Buffering Control Strategies

This section will discuss various regulatory and advanced buffering pressure control techniques. Not all the variations for each type of control scheme will be investigated but rather a representative formulation chosen from the available literature. Information regarding the stability and robustness requirements for the various control schemes may be found in the respective reference material and will not be repeated in this work.

4.1. Cascaded Flow Strategies

It is important when designing a pressure control scheme to consider if the pressure control outputs are directly sent to the final control element such as a control valve or compressor speed, or sent to a flow controller in a cascade control scheme. Additionally, the linearisation and prioritisation of the slave controllers have to be considered. This section discusses some regulatory pressure-flow cascade schemes relevant to pressure header control.

4.1.1. Flow Cascade Control

The main advantage of using flow cascade control is that the slave controller is able to detect and resolve any local disturbances before the error of the master controller is affected. The requirement is that the dynamics of the slave controller are considerably faster than the master controller [20, 22]. The header pressure will change at almost the same time as the flow into or out of the header and therefore it appears that there is no dynamic advantage for cascade flow control. However, for averaging or buffering control there are additional advantages to using a cascade scheme. This is that local disturbances around the final control element such as upstream or downstream pressure changes can be compensated for quickly to maintain a constant flow. To achieve this without a cascade scheme the pressure would have to be tuned tightly which is in contradiction with the buffering control objectives. Therefore, cascade flow control augments the buffering control ability of a given control scheme.

4.1.2. Total Flow Linearisation

The purpose of total flow linearisation is to reject local disturbances related to the mass balance closure of numerous parallel slave flow controllers. This is often used where parallel trains of processing units supply or pull out of the same header such as the compressors treated as a single compressor in Fig. 9. The other purpose of the total flow controller is to linearise the overall response of the slave controllers, i.e., the gain of the pressure controller remains constant irrespective of the amount of parallel slave controllers in cascade with the total flow controller.

One method is to use an integral-only (I-only) controller as a total flow controller illustrated in Fig. 3. The SP to the total flow controller is the output (OP) received from the master pressure controller and the process value (PV) of the total flow controller is a summation of all the slave flow controller SPs pulled from the individual slave controller points indicated by the blue dotted lines. The OP of the total flow controller is sent

to the flow slave controller SPs. Therefore, the total flow controller will through feedback correct the mass balance for any disturbances in the slave control loops such as process trips, removing slave loops from cascade, or other control schemes taking control of slaves through an override. The integral tuning is used to determine the speed at which the cascaded slaves respond to a disturbance in the SP of a specific slave. The integral time is usually fast (1 second). This is not a concern in terms of closed loop stability since the total flow control feedback loop does not contain any process dynamics. This is because the PV of the master flow controller is the summation of the slave SPs.

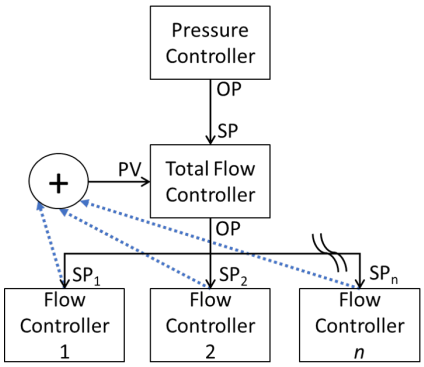

Figure 3: Total flow linearisation.

Alternatively, the slave flow controller SPs can be explicitly calculated which eliminates the small lag introduced by the I-only controller. This calculation requires more computing power and memory on the distributed control system (DCS), and more calculations steps which increases the maintenance of the loop. Therefore, there is a trade-off between the space available on the DCS and the maintenance requirements and the small phase lag introduced by the fast integral time in the I-only controller.

4.1.3. Multiple-Input-Single-Output

Pressure headers are often multiple-input-single-output (MISO) systems because multiple streams can be used to influence the pressure as the only controlled variable. A detailed discussion or comparison of MISO systems is outside the scope of this study. However, it is beneficial to describe briefly the specific application of MISO schemes to pressure header control used in this work. The MISO control scheme applied is deviation control and is used as the MISO control strategy of choice. This is the existing scheme used on the industrial case study header in Section 6. Other MISO strategies not used or discussed in this work are: split range, staggered, and position control [37, 39].

To illustrate how the MISO control scheme interfaces with the process, an example is used where a consumer valve, a flare valve and an expensive supplier valve are available as manipulated variables (MVs). This configuration is similar to Fig. 2 and comparable with the industrial case study shown in Fig. 9 without an expensive consumer valve. Additionally, it is assumed that flow measurements are available so that cascaded flow controllers may be used to manipulate the valves. Therefore, PV inputs to flow controllers are from flow measurements in the process and PV inputs to pressure controllers are from the chosen pressure measurements in the process.

Deviation control as shown in Fig. 4 is based on the mass balance principle. The deviation controller works by opening the flare or the expensive supplier when there is a deviation between the OP of the pressure controller to the flow controller and the SP received by the flow controller. The flare and expensive supplier controllers will react if the consumer flow controller (SP_V) deviates from the value required by the pressure controller (OP_P). In Fig. 4 the flare controller will open when the consumer flow controller is limited by the high limit (HL) block through the selector (<) and the expensive supplier controller will open when the consumer flow controller is limited by the low limit (LL) block through the selector (>).

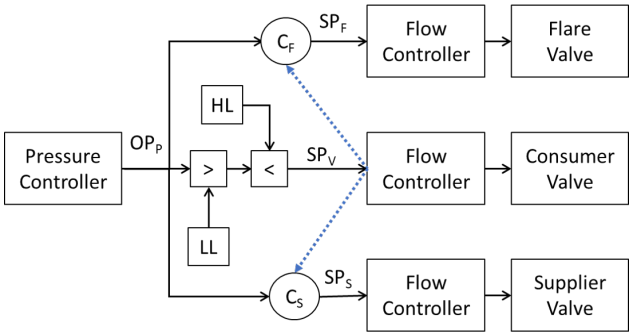

Figure 4: Deviation Control.

The calculations done in C_F and C_S are shown in (15a) and (15b) respectively.

$$SP_F = \max\{OP_P - SP_V, 0\}, \tag{15a}$$

$$SP_S = \max\{SP_V - OP_P, 0\}. \tag{15b}$$

SP_F is the signal from the C_F block to the flare flow controller, SP_S is the signal from the C_S block to the expensive supplier flow controller, OP_P is the output from the pressure controller, and SP_V is the SP received by the consumer flow controller. SP_V is sent to C_F and C_S from the flow controller as indicated by the dotted blue lines in Fig. 4. As shown in (15) the output to the flare and expensive supplier flow controllers are limited to be ≥ 0.

This scheme is commonly used when there are overrides which can limit or cut back the process valve at different operating regions indicated by the HL and LL blocks in Fig. 4. The consumer flow controller SP (SP_V) is directly pulled from the flow controller and not from a selector block output so that scenarios such as initialisation, wind-up or downstream mode changes can be captured. Deviation control can be seen as a special case of split-range control [39].

The combination of total flow controllers and MISO control strategies are useful to improve local disturbance rejection and prioritise MVs to help satisfy buffering control objectives in the regulatory control layer. Subsequent sections will focus on the pressure buffering controller algorithm and assumes a suitable cascade pressure-flow control strategy is in place.

4.2. Regulatory Pressure Control

Regulatory techniques provide a baseline for comparing more advanced control strategies, can be used as suitable fall-back strategies, and may provide close to optimal operation with reduced complexity when compared with advanced applications [19, 29, 40].

The process model used for the tuning rules is derived from (5c) as,

$$\frac{dP}{dt} = \frac{ZR\,T}{ALM_w}\Big(Q_{in} - Q_{out}\Big). \tag{16}$$

The derivation of (16) from (5c) is shown in Appendix A.2. The process gain of the integrating pressure header process is approximated as,

$$K \approx \frac{ZR\,T}{ALM_w}, \tag{17}$$

and is independent of the pressure measurement location on the pipe [37].

It is useful to contrast (16) with the standard tank model used in averaging level control studies to show the increase in variables,

$$\frac{dh}{dt} = \frac{1}{a}\Big(Q_{in} - Q_{out}\Big). \tag{18}$$

h is the level height and a the tank cross sectional area. The similarities between (16) and (18) are used in this study to adapt the averaging level control schemes found in literature for pressure buffering control. It should be noted that a may contain non-linearities due to the vessel geometry that may be accurately compensated for with signal conditioning.

4.2.1. PI Control

PID controllers may vary in their exact implementation depending on the application. The typical solution to pressure control is the standard PI controller represented in discrete velocity form as [22],

$$\Delta\mathcal{M} = \mathcal{M}_k - \mathcal{M}_{k-1} = K_c\Big[(E_k - E_{k-1}) + \frac{t_k - t_{k-1}}{\tau_I}E_k\Big], \tag{19}$$

where E_k is the error defined as $E_k = PV_k - SP_k$, K_c is the controller gain, τ_I is the integral time, and $\mathcal{M}_k$ is the buffering controller output at time step k.

The drawback of standard PID control is that control action is always taken to reach SP. This is counterproductive when applied to buffering control. A solution might be to relax the tuning on the PID controller, but this increases the risk of violating process constraints. Tuning heuristics have been proposed in literature [19, 20, 21, 22, 23, 24, 29, 33] to provide PID tuning constants specifically for tank level buffering without violating constraints. Derivative action is typically used for SP tracking and is therefore not used for pressure buffering control.

4.2.2. IMC PI Tuning Rules

Standard PI control tuned for SP tracking will be used as a baseline controller. The IMC tuning rules for integrating processes with a 15% overshoot for SP changes are [20],

$$K_c = \frac{2\lambda + \theta}{K(\lambda + \theta)^2}, \tag{20a}$$

$$\tau_I = 2\lambda + \theta, \tag{20b}$$

$$\lambda = 0.31\theta + 0.88\tau_P, \tag{20c}$$

where τ_P is the process lag time constant determined empirically, θ is the process dead time, K_c is the PI controller gain, and τ_I is the PI controller time constant.

4.2.3. SIMC PI Tuning Rules

In this work the SIMC tuning rules for integrating processes suggested by [19] will be applied to a standard PI controller for buffering control. The SIMC rules proposed are as follows,

$$K_c = \frac{1}{K(\tau_c + \theta)}, \tag{21a}$$

$$\tau_I = 4(\tau_c + \theta). \tag{21b}$$

Following the reasoning in [19], K_c will be chosen and used to solve for $\tau_c + \theta$ which is then used to solve for τ_I. The controller gain is chosen as [37],

$$K_c = \frac{Q_{max}}{P_{max}}, \tag{22}$$

from which τ_c and τ_I can be solved using (21). Q_{max} is the maximum allowed manipulated flow rate deviation from the initialised value and P_{max} is the maximum allowed pressure deviation from SP at the chosen measurement location.

4.2.4. Piecewise-Linear Control

An intuitive, and often applied solution to the contradiction between PID control and buffering control is to only take action when the error has reached a certain magnitude, thereby taking less or zero action when the PV is close to the SP. These piecewise-linear techniques are intended to capture the advantages of nonlinear averaging level control while also providing easier tuning and improved predictability [25]. Some variations of this method include proportional-integral/iroportional (PIP), dual range integral/proportional (DRIP), and gap control [20, 25]. Gap control is widely used in industry and will be used in this work where the controller gain is calculated as [20],

$$K_c = \begin{cases} \frac{Q_{max}K_r}{(P_{max} - (1-K_r)g)} & E < g, \\ \frac{Q_{max}}{(P_{max} - (1-K_r)g)} & E \geq g. \end{cases} \tag{23}$$

The gap ratio K_r and gap size g are design choices with $K_r = 0.5$, $g = \frac{P_{max}}{2}$, and τ_I as in (21). K_r determines the reduction in proportional action taken. The choice of g determines the gap size and allows for reduced action to be taken for small disturbances where the error (E) remains smaller than g and more action taken for large disturbances where E is greater than or equal to g.

There are however drawbacks to piecewise-linear control implementations in the form of non-linearities introduced into the closed-loop control action at the discontinuous boundaries.

These non-linearities are proportional to the difference in magnitude of the changing piece-wise term (K_c in (23)) when inside or outside the gap. The non-linearities may lead to cycling in the control action which is unwanted for consumer stability. Piecewise-linear control is best suited to when the disturbances can be classified into two distinct groups of small and large disturbances [20].

4.2.5. Range Control

Range control is a similar approach to gap control and is achieved without introducing non-linearities. Range control makes use of two or three PID controllers in conjunction with a mid-of-three (MO3) selector logic block. There are numerous configurations which can be built around the MO3 block, some of which include:

- Two PI range controllers as inputs to the MO3 block with the third input as the output from the MO3 selector block. This scheme does not have a SP between the high and low limits.
- Three P controllers as inputs to the MO3 block, with two range controllers tuned aggressively and one tuned for averaging control. This configuration does not perfectly return to SP [19].
- Two P-only range controllers as inputs with a PI controller as a third input to the MO3 block [19].
- Three PI controllers with two aggressively tuned range PI controllers and one PI controller tuned using averaging control methods as inputs to the MO3 block.

The last method with three PI controllers will be used in this work. It should be noted that the range control scheme only utilises the consumer flow rate (Q_v in Fig. 2) similar to all the other control schemes in Section 4.2. The control structure is shown in Fig. 5.

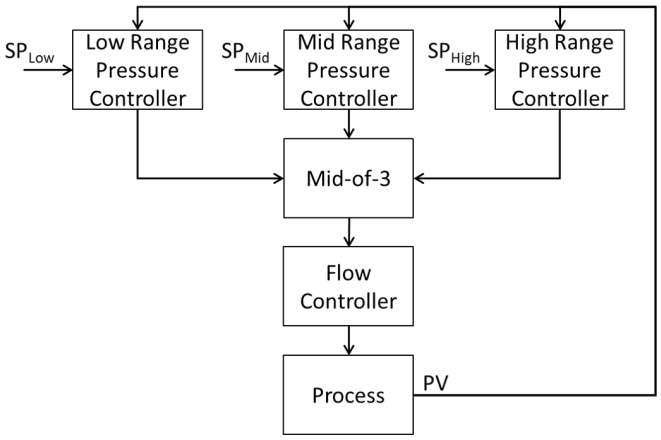

Figure 5: Mid-of-three selector logic block with high range, low range, and mid range pressure controllers.

The tuning for the mid range controller gain and all the time constants are obtained as specified by (21), and the gains for the low range and high range controllers are adapted from the tight level control heuristics given in [20] for header pressure control in this work as,

$$K_c = \frac{0.4}{KQ_{max}}. \tag{24}$$

This method requires an anti-reset windup scheme configured on all the PI controllers [22, 41]. More specifically, (19) becomes,

$$\Delta\mathcal{M} = K_c\Big[(E_k - E_{k-1}) + \frac{\Delta t}{\tau_I}E_k\Big] + \frac{\Delta t}{\tau_I}(R_F - \mathcal{M}_{k-1}), \tag{25}$$

where R_F is the reset feedback signal which is set equal to the PV of the flow controller. The units of R_F should be the same as $\mathcal{M}$.

4.2.6. Error-squared PID Control

A popular non-linear algorithm used in industry is the error-squared algorithm which can be used in a stand-alone manner or in conjunction with a PID control algorithm [20, 21, 22, 27, 41]. There are numerous implementation methods, one of which is [20],

$$\Delta\mathcal{M} = K_c|E_k|\left[(E_k - E_{k-1}) + \frac{\Delta t}{\tau_I}E_k\right]. \tag{26}$$

The addition of the $|E_k|$ term aims to enhance the performance of the controller by increasing the effective gain as the error increases. Similar to gap control this algorithm exhibits oscillatory behaviour. As an improvement, the term C can be incorporated to allow a design choice of weighing the influence of the error-squared term in the PID algorithm as,

$$\Delta\mathcal{M} = K_c(C|E_k| + 1 - C)\left[(E_k - E_{k-1}) + \frac{\Delta t}{\tau_I}E_k\right]. \tag{27}$$

The controller tuning is adapted from [20] for the error-squared form in (27) as,

$$K_c = \frac{Q_{max}}{P_{max}}\frac{2}{2(1-C) + \frac{C}{P_{max}}}, \tag{28}$$

with C chosen as 0.9 and τ_I as in (21). The error-squared algorithm structure will not have a large impact on the control performance but the tuning of K_c in (28) will change if the algorithm structure changes [20].

4.2.7. Polynomial Averaging Control

An averaging level control algorithm is proposed by [28] where a non-linear fourth-order polynomial term is used to adjust the controller output to keep a tank level within limits while minimising output movement. To be specific, this technique will be called polynomial averaging control in this work. The polynomial is defined as,

$$g(x) = a_1x + a_2x^2 + a_3x^3 + a_4x^4, \tag{29}$$

such that,

$$g(1) = 1 \qquad \implies a_1 + a_2 + a_3 + a_4 = 1, \tag{30a}$$

$$g(\bar{x}) = \bar{u}_o \qquad \implies a_1\bar{x} + a_2\bar{x}^2 + a_3\bar{x}^3 + a_4\bar{x}^4 = q + 0.5, \tag{30b}$$

$$\frac{dg}{dx}(\bar{x}) = s \qquad \implies a_1 + 2a_2\bar{x} + 3a_3\bar{x}^2 + 4a_4\bar{x}^3 = s, \tag{30c}$$

$$\frac{d^2g}{dx^2}(\bar{x}) = 0 \qquad \implies 2a_2 + 6a_3\bar{x} + 12a_4\bar{x}^2 = 0. \tag{30d}$$

The parameters if adapted for pressure control are,

$$\bar{x} = 0.5 + qd, \tag{31a}$$

$$\bar{u}_o = \frac{Q_{out} - \underline{Q}_{out}}{\bar{Q}_{out} - \underline{Q}_{out}}, \tag{31b}$$

$$x = \frac{P_R - \underline{P}_R}{\bar{P}_R - \underline{P}_R}, \tag{31c}$$

$$q = \frac{Q_{AVG} - \underline{Q}_{in}}{\bar{Q}_{in} - \underline{Q}_{in}} - 0.5. \tag{31d}$$

(30) is used to solve the polynomial constants (a_1, a_2, a_3, a_4) as functions of q by choosing design values for the relation between the average pressure and average flow (d), and the desired slope at the inflection point (s), such that,

$$g(x, q) = a_1(q)x + a_2(q)x^2 + a_3(q)x^3 + a_4(q)x^4. \tag{32}$$

The average inlet flow rate (Q_{AVG}) can be calculated online using a low pass filtered value of the uncontrolled inlet flow rate (Q_{in}). The final control equation is,

$$\mathcal{M} = Q_{out} = \underline{Q}_{in} + g\Big(x, q\Big)(\bar{Q}_{in} - \underline{Q}_{in}), \tag{33a}$$

where the measured input pressure (P_R), and the average inlet flow (Q_{AVG}) are the inputs and the controlled outlet flow rate (Q_{out}) is given in positional form. In this work $s = 0$ and $d = 0.5$.

4.2.8. Variable Set-Point PI Control

A method is proposed by [29] where the SP of the pressure PI controller is moved to loosely track the pressure measurement PV as given by an inlet flow (Q_{in}) dependent affine mapping,

$$\text{SP} = K_{SP}Q_{in} + b_{SP}, \tag{34}$$

where K_{SP} and b_{SP} are parameters which are adapted from [29] for pressure control as,

$$K_{SP} = \frac{\bar{P}_R - \underline{P}_R)}{(\bar{Q}_{in} - \underline{Q}_{in})}, \tag{35}$$

$$b_{SP} = \frac{(\bar{Q}_{in}\underline{P}_R - \underline{Q}_{in}\bar{P}_R)}{(\bar{Q}_{in} - \underline{Q}_{in})}. \tag{36}$$

By moving the SP intelligently, the PI algorithm is implicitly exploited to provide buffering control. This formulation is designed to replicate the predictive behaviour of an MPC by adapting the PI controller SP when the mass balance changes. When the optimal level control tuning rules given by [29] is adapted for pressure control, the PI tuning becomes,

$$K_c = \frac{4}{K\tau_I}, \tag{37a}$$

$$\tau_I = \frac{6K_{SP}}{5K}. \tag{37b}$$

4.3. Feed-forward Control

It is tempting to incorporate standard additive feed-forward signals from the uncontrolled flow streams into the pressure control scheme. This will inevitably aid in closing the mass balance and improve the header pressure control in terms of SP deviation. However, adding standard feed-forward signals on the regulatory control level will negatively impact the buffering control performance as the feed-forward contribution will aim to resist deviations from the pressure SP and add contributing movements to the cascaded flow controllers thereby negatively impacting consumer stability and flaring.

There are examples where feed-forward signals are effectively used in advanced regulatory schemes (e.g. Sections 4.2.7 and 4.2.8). Feed-forward signals in the form of disturbance variables (DVs) do not suffer from the same shortcomings when incorporated into MPC schemes as the pressure range can be defined as slack variables. Therefore, the MPC predictions will be able to exploit the feed-forward signal in aiding the buffering control objectives by optimally using the available buffering capacity.

4.4. Model Predictive Pressure Control

The regulatory control techniques discussed in Section 4.2 mostly rely on feedback and tuning to accomplish the buffering control objective. MPC is an attractive and widely accepted solution which may further improve the buffering utilisation in the presence of non-linearities. MPC applications are attractive due to the potential use of non-linear models, predictive capabilities, and the implicit use of objective functions.

For MPC applications, the states in (7) and the model outputs in (13) can be discretised into $\mathcal{N}_P$ elements as,

$$\begin{aligned} \boldsymbol{x}_{k+j} &= \boldsymbol{f}(\boldsymbol{x}_{k+j-1}, \boldsymbol{u}_{k+j-1}) \quad \forall\ j \in [1, \mathcal{N}_P], \\ \boldsymbol{y}_{k+j} &= \boldsymbol{g}(\boldsymbol{x}_{k+j}, \boldsymbol{u}_{k+j}) \quad \forall\ j \in [1, \mathcal{N}_P]. \end{aligned} \tag{38}$$

The objective function to minimise is defined in this study for pressure buffering control as,

$$\begin{aligned} \min_{\boldsymbol{u}} \Bigg[& \sum_{j=1}^{\mathcal{N}_P} \Big(\|E_{k+j}\|^2 W_P + \|s_j\|^2 W_S \Big) + \\ & \sum_{j=0}^{\mathcal{N}_C - 1} \Big(\|\Delta \boldsymbol{u}_{k+j}\| W_C + \boldsymbol{u}_{k+j} W_L \Big) \Bigg], \end{aligned} \tag{39}$$

subject to,

$$\underline{\boldsymbol{y}} \le \boldsymbol{y}_{k+j} \le \bar{\boldsymbol{y}} \quad \forall\ j \in [0, \mathcal{N}_P], \tag{40a}$$

$$\underline{\boldsymbol{u}} \le \boldsymbol{u}_{k+j} \le \bar{\boldsymbol{u}} \quad \forall\ j \in [0, \mathcal{N}_C - 1], \tag{40b}$$

$$\Delta\underline{\boldsymbol{u}} \le \Delta\boldsymbol{u}_{k+j} \le \Delta\bar{\boldsymbol{u}} \quad \forall\ j \in [0, \mathcal{N}_C - 1]. \tag{40c}$$

W_P, W_S, W_C, and W_L are weighting matrices for the output reference error, slack variables, input move sizes and, input magnitudes respectively. The weighting matrices used for the MPC controllers in this study are shown in Appendix B. $\mathcal{N}_P$ is the prediction horizon and $\mathcal{N}_C$ is the control horizon defined as

$\mathcal{N}_C = \mathcal{N}_P/2$. E_{k+j} are deviations from the desired output trajectory and s_j are the slack variables used to penalised output constraint violations. $\underline{\boldsymbol{y}}$ and $\bar{\boldsymbol{y}}$ are the output low and high limits, $\underline{\boldsymbol{u}}$ and $\bar{\boldsymbol{u}}$ are the input low and high limits, and $\Delta\underline{\boldsymbol{u}}$ and $\Delta\bar{\boldsymbol{u}}$ are the change in input low and high limits. SP tracking, pressure limits and MV move sizes are included as optimisation objectives in (39). Controlled variable (CV) ranges are included as hard constraints (40a), MV ranges are included as hard constraints (40b) and MV move sizes are included as hard constraints (40c) to meet process stability constraints.

The solution of (39) is a set of proposed future $\mathcal{V}$ input moves,

$$\boldsymbol{u}^{\mathcal{V}} = (u_k, u_{k+1}, \ldots, u_{k+\mathcal{V}-1}), \tag{41}$$

of which the first move is executed in velocity form as,

$$\Delta\mathcal{M} = u_k - u_{k-1}. \tag{42}$$

Although the objective is to keep the pressure between limits for buffering control, it is desirable to slowly move the pressure towards the SP between the limits with the penalty W_P so that sequential disturbances in the same direction can be rejected. Consumer stability is optimised through the input move size weights W_C. The expensive supplier and flare flow magnitudes are minimised with the weights W_L. In practice MPCs applied to industrial gas headers have to execute at fast time intervals to respond accurately to the fast gas dynamics. The simulated and real-world MPCs in this study execute at 6 second intervals.

In this study, the MPC formulation remains the same and only the respective models and required inputs used for the predictions change, namely: linear MPC (LMPC), non-linear MPC (NMPC), and compensated linear MPC (CLMPC). LMPC is discussed in Section 4.4.1, NMPC is discussed in Section 4.4.2, and CLMPC is discussed in Section 4.4.3.

4.4.1. Linear Model Predictive Control

A linear model is required for linear LMPC applications and is described as,

$$\delta\dot{\boldsymbol{x}} = A\delta\boldsymbol{x} + B\delta\boldsymbol{u}, \tag{43a}$$

$$\delta\boldsymbol{y} = C\delta\boldsymbol{x} + D\delta\boldsymbol{u}, \tag{43b}$$

This formulation is obtained from the nonlinear equations of Section 3 by obtaining the first order Taylor series expansion of the functions $\boldsymbol{f}(\boldsymbol{x},\boldsymbol{u})$ and $\boldsymbol{g}(\boldsymbol{x},\boldsymbol{u})$ in (14) with respect to $\boldsymbol{x}$ and $\boldsymbol{u}$ at a chosen steady state operation $\boldsymbol{x} = \boldsymbol{x}_0$ and $\boldsymbol{u} = \boldsymbol{u}_0$. The deviation variables are defined as $\delta\boldsymbol{x} = \boldsymbol{x} - \boldsymbol{x}_0$, $\delta\boldsymbol{u} = \boldsymbol{u} - \boldsymbol{u}_0$, and $\delta\boldsymbol{y} = \boldsymbol{y} - \boldsymbol{y}_0$. The matrices A, B, C and D for the equilibrium condition in Table 1 are shown in Appendix A.1. The LMPC in this study assumes that Z, T, and M_w are constants with values at the linearised conditions. The LMPC model inputs are given by the input vector $\boldsymbol{u}$ as,

$$\boldsymbol{u} = [Q_z, Q_L]^T. \tag{44}$$

4.4.2. Non-linear Model Predictive Control

The model in (6) is conveniently already in state-space format and can be used in a NMPC framework. The advantage of the NMPC formulation above the LMPC formulation in this study is that the NMPC is not linearised at a chosen steady-state and does not assume constant parameters. This allows the NMPC prediction to capture the non-linear properties of gas with respect to temperature, pressure and composition. Therefore the NMPC model inputs are given by the input vector $\boldsymbol{u}$ in (44) and the time-updated parameter vector $\boldsymbol{p}$,

$$\boldsymbol{p} = [M_w, Z,\ T]^T, \tag{45}$$

where the parameters M_w, Z, and T are calculated or inferred at each time step from process inputs [38].

4.4.3. Compensated Linear Model Predictive Control

The state-space models used by the LMPC and NMPC applications in this study are large $2(nN+1)$ order models and cumbersome to use in industrial applications. As an example, using the parameters in Table 1 result in a 14^{th} order LMPC model. In practice, it is desirable to have accurate low order plant models which can be used in a linear solver. To this end, a compensated linear model is developed and used within a LMPC framework. This is called CLMPC in this study.

Using a suitable model order reduction technique [42, 43, 44], the model in (43) can be reduced to a second order model. A second order reduced model is chosen as it can capture the process lags and potential inverse responses observed in gas headers [37]. An optimal Hankel norm approximation [42] was used in this work to produce low order models which correspond well to the original high order model predictions. The reduced model is written as a Laplace domain transfer function, $\hat{G}(s)$. $\hat{G}(s)$ is the plant model whereby the two inputs, Q_z and Q_L, are related to the chosen pressure output obtained through (13). Each sub-model in $\hat{G}(s)$ has the following structure,

$$\frac{K'(\tau_1 s+1)(\tau_2 s+1)}{s(\tau_3 s+1)(\tau_4 s+1)}, \tag{46}$$

where τ_1, τ_2, τ_3, and τ_4 are the reduced model response time constants and K' is the integrating process gain. The model structure in (46) can easily be used in an industrial DCS or model-based framework such as MPC.

Fig. 6 compares the unit step response and Fig. 7 compares the frequency plot of the high order linear model (43) to the reduced model (46). It can be seen that the reduced model sufficiently represents the original high order model.

Due to numerical errors, it is sometimes required during model reductions to first reduce the original state-space model into a self-regulating third order system with two lead terms and subsequently remove the denominator polynomial intercept term to transform the model into a second order integrating model. In this case, the removed term is negligibly small due to the integrating nature of gas headers as shown in Appendix A.1.

CLMPC aims to leverage the non-linear prediction capability of NMPC while at the same time benefiting from the reduced complexity of using LMPC. The CLMPC approach measures or infers Z, T, and M_w from available measurements at the pressure measurement location (P_R), and calculates the ratio

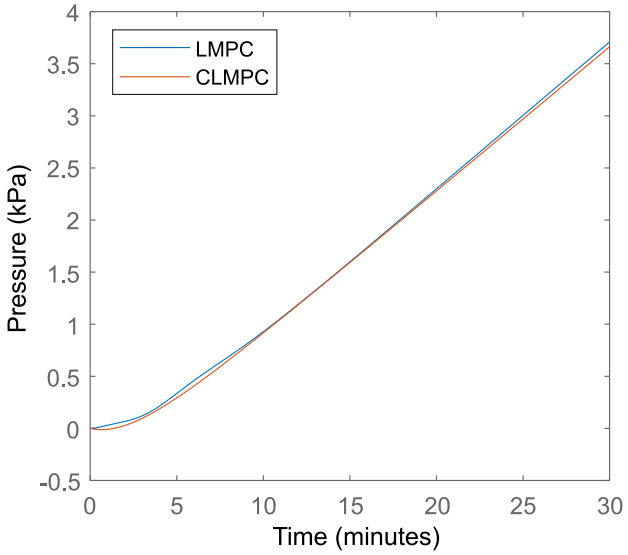

Figure 6: Responses of the reduced (CLMPC) and high order (LMPC) model pressures given a step disturbance to the inlet flow rate (Q_D) of unit magnitude.

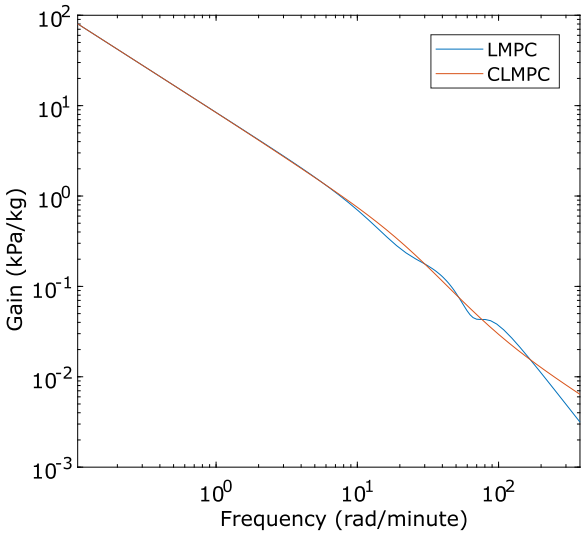

Figure 7: Frequency plot of the reduced (CLMPC) and high order (LMPC) models.

between the calculated gain in (17) and the gain used in the approximated linear model (46) as,

$$K_p = \frac{K}{K'}, \tag{47}$$

where K_p is the gain multiplier calculated in real time. The final model used in the CLMPC framework is,

$$K_p K' \frac{(\tau_1 s + 1)(\tau_2 s + 1)}{s(\tau_3 s + 1)(\tau_4 s + 1)}. \tag{48}$$

K' is inherent to the controller design and cannot simply be replaced during online operation. Therefore, K' is adjusted using the gain multiplier K_p. CLMPC is promising because of the integrating nature of the header pressures. This is because the non-linearity exists mostly in the slope of the integrating response and variations in the phase lead and lag dynamics have negligible contributions to the design of a controller with integrating dynamics [37, 44]. The integrating response of gas headers can be seen in Fig. 6. Additionally, if the parameter dynamics observed in Z, T, and M_w are sufficiently slower than the controller execution frequency, then the CLMPC approach will be able to perform similar to the NMPC approach. The reason this is useful in industry is because most of the existing industrial control packages are linear model predictive controllers and can use model structures similar to (46).

CLMPC can be used to augment existing linear controllers by adjusting the gain of the integrating model without changing the inherent design and realising some of the non-linear controller benefits. Therefore, this method may be applied to controllers derived using auto regressive with exogenous inputs (ARX) and finite impulse response (FIR) models as only the gain is compensated with (47).

5. Comparison of Control Schemes

A simulation of the plant shown in Fig. 2 is used to compare the different control schemes discussed in Section 4. A buffering pressure controller is used to control Q_V, an under pressure controller is used to control Q_S during low pressure scenarios, and an over pressure controller is used to control Q_F during high pressure scenarios [37]. The buffering controller is altered based on the controller being evaluated. For the regulatory control schemes of Section 4.2, the over and under pressure controllers are configured using the deviation control scheme (Fig. 4). The MPC schemes in Section 4.4 manipulate all the available streams directly. P_R is measured at the centre of the header - this corresponds to location P_4 in (8a). The simulation model parameters are given in Table 1.

Section 5.1 compares the various proposed control schemes using a Monte Carlo simulation. The control schemes are compared in parallel for each Monte Carlo scenario, i.e., the control schemes are simulated for the same time horizon per simulation. A sensitivity analysis is conducted on the non-linear model parameters in Section 5.2 to quantify the individual contribution of the gas properties to the total cost calculated in Section 5.1.

5.1. Simulation

The gas header pressure responses are sensitive to changes in the nominal parameters shown in Table 1. A Monte Carlo simulation is performed to sample the expected parameter variation space.

A sinusoidal load disturbance is injected into the system through Q_D in Fig. 2 to evaluate the cost functions. The disturbance sine wave amplitude is changed to capture small, typical, and large disturbance magnitudes. The sine wave period is changed to capture fast, medium and slow disturbance frequencies. Additionally, the gas properties $P_{z,0}$, T, M_w, and Z are varied to simulate operating region variations due to factory

operational changes. The disturbance and parameter variation ranges have a uniform distribution as given in Table 2. The parameter ranges are selected based on typical parameter variations observed in the industrial case study process described in Section 6.

Table 2: Monte Carlo simulation disturbance parameters and variation ranges.

Parameter	Range	Units
Compressibility (Z)	0.95 - 1	-
Temperature (T)	295-330	K
Molecular Weight (M_w)	17 - 20	kg/kmol
Initialising Inlet Pressure ($P_{z,0}$)	1800 - 3400	kPa
Disturbance Magnitude	2.5 - 7.5	kg/s
Disturbance Sine Wave Period	1 - 60	min

The Monte Carlo simulation is setup as follows:

1. Randomly generate $\mathcal{S}$ scenarios sampled from the ranges in Table 2. $\mathcal{S}$ is chosen as 2500 to achieve repeatable results.
2. Initialise and run the simulation for each of the $\mathcal{S}$ scenarios where each scenario is allowed to run for two periods determined by the selected sine wave period.
3. Determine the cost of flaring, supplier use, and consumer stability using (2) for each control technique per scenario.
4. Determine the total cost of flaring, supplier use, and consumer stability across all scenarios.

As a representative example of the simulations, Fig 8 shows a simulation run using the median values of the ranges in Table 2 with the exception of the disturbance magnitude. The disturbance magnitude is given a value of 7.5 to showcase the flaring and expensive supplier use by forcing more gas into the header than the consumer can accommodate. A PI controller tuned using the standard SIMC rules in Section 4.2.3 is used in Fig 8a, a range controller described in Section 4.2.5 is used in Fig 8b, and a NMPC controller described in Section 4.4.2 is used in Fig 8c.

Table 3 gives the cost values of each controller across all Monte Carlo simulations as well as a measure of controller complexity. Complexity is measured in this study by comparing the number of process outputs (NPO) to the controller as inputs, and number of tuning parameters (NTP) per control scheme. SPs are not considered process outputs or tuning parameters. Additionally, parameters and weights with a value of zero, such as derivative time constants, and unused MPC weights are not considered.

The cost of consumer stability (J_V) is normalised relative to the PI controller tuned with IMC rules as this is the worst case for consumer stability. The controller cost of flaring (J_F) and expensive supplier use (J_S) are normalised relative to an override only controller. The override only scheme refers to when the pressure is only controlled between limits by the over and under pressure controllers and the buffering control scheme is

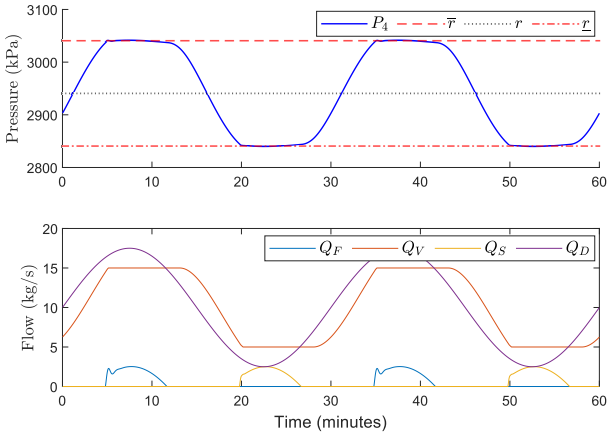

(a) SIMC controller.

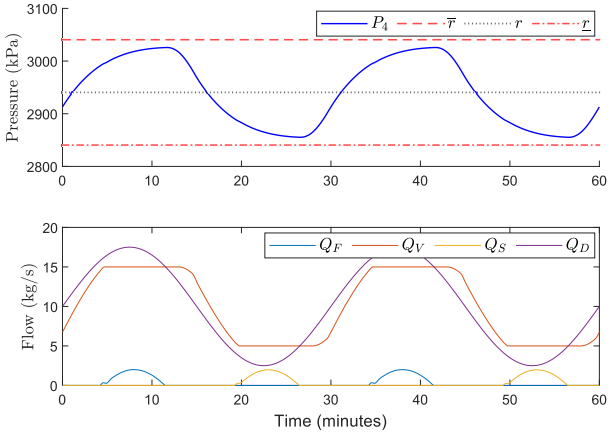

(b) Range controller.

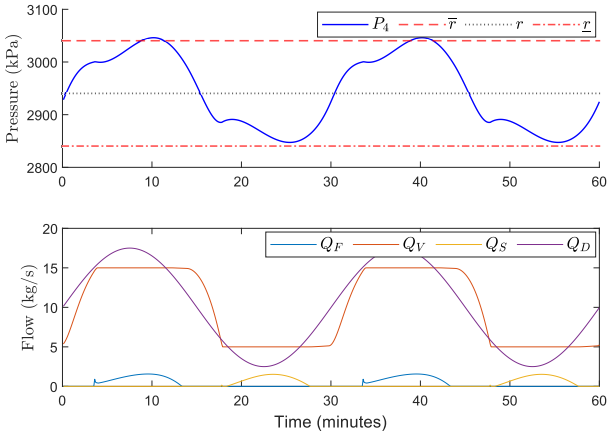

(c) NMPC controller.

Figure 8: Example simulations of the SIMC, Range and NMPC controllers using the median of the process parameters in Table 2 and a disturbance magnitude of 7.5 kg/s.

disabled, i.e., the buffering controller output (Q_V) is constant at the initialised value.

Table 3: Cost of flaring (J_F), supplier use (J_S), and consumer stability (J_V) results accross all Monte Carlo simulations. The number of tuning parameters (NTP) and process outputs (NPO) are also shown.

Controller	$J_F + J_S$	J_V	J_T	NTP	NPO
Overide Only	100	0	100	2	1
PI (IMC) (4.2.2)	7.9	100	107.9	2	1
PI (SIMC) (4.2.3)	23.5	82	105.5	2	1
Gap (4.2.4)	19.7	85.6	105.3	3	1
Range (4.2.5)	17.2	81.1	98.2	6	2
Error-Squared (4.2.6)	20	82.9	102.9	3	1
Polynomial (4.2.7)	20.4	83.8	104.2	2	2
Variable SP (4.2.8)	22.3	82.9	105.1	3	2
LMPC (4.4.1)	16.2	82	98.1	7	4
NMPC (4.4.2)	15.7	81.1	96.7	7	7
CLMPC (4.4.3)	16	82	97.9	7	7

From Table 3 the following observations are made:

- In terms of total cost (J_T), the PI controllers have the worst performance. The advanced regulatory controllers such as gap, range, and error squared have improved performance over the basic PI controllers. The MPC controllers have the best performance.
- Notably, the range control scheme outperforms the other advanced regulatory schemes and has similar performance to the MPC schemes. However, the range control scheme has a greater number of NTP and NPO than the other base-layer schemes.
- The NMPC scheme has the best overall performance followed by the CLMPC scheme.
- There is a relationship between the controller performance and complexity. In general, the higher the number of NTP and NPO, the lower the total cost (J_T).
- The override scheme seems to perform well in terms of total cost (J_T). However, this is dependant on the individual contributions of J_1, J_2, and J_3 in (2). If these costs are weighed more heavily towards emissions and expensive supplier use, it would perform badly compared to all the other controllers.
- The polynomial and variable SP controllers performed poorer than expected in gas headers. This is due to the feed-forward signals used in these schemes not taking the lag dynamics of gas headers into account which results in over compensation. Therefore, the controllers do not achieve a similar performance improvement when used in a like-for-like implementation in gas headers as they are applied to buffering tanks. However, the controllers still performed well when compared to standard PI and gap control and further improvement may be possible if the feed-forward signals include lag dynamics.

5.2. Gas Property Sensitivity Analysis

It is beneficial at this stage to examine the impact of the individual gas properties on the non-linear model variance as the gas property values influence the regulatory control tuning and are used as inputs in the NMPC and CLMPC schemes. To this end, a variance based global sensitivity study is done by computing the first- and total-order Sobol indices [45]. The first-order Sobol indices give the fraction of the overall response variance that can be attributed to variations in the input parameter alone. The total-order indices give the fraction of the overall response variance that can be attributed to any joint parameter variations that include variations of the input parameter.

The Sobol indices are evaluated on the total cost (J_T) as an output from the Monte Carlo simulation environment in Table 3. The nominal values are given in Table 1 and the gas properties to be analysed are $P_{z,0}$, T, M_w, and Z given the ranges in Table 2. The Sobol indices are evaluated in the Monte Carlo simulation environment as discussed in Section 5.1. The results are shown in Table 4.

Table 4: First- and total-order Sobol indices.

Parameter	First-order Effects	Total-order Effects
Z	0.069	0.066
T	0.32	0.33
M_w	0.61	0.63
$P_{z,0}$	0.023	0.0

The sensitivity study was conducted at the varying disturbance sine wave periods and disturbance magnitudes in the ranges given in Table 2. However, the difference in the Sobol indices at different periods and magnitudes is negligibly small. Therefore, the averaged Sobol effects across the varying periods and disturbances are displayed in Table 4.

It can be seen from Table 4 that M_w has the largest influence on the total cost. T has the second largest effect followed by Z. $P_{z,0}$ has a very low influence on the total cost. The results obtained are dependant on the parameter ranges specified in Table 2 and the type of distribution assigned to each parameter. Therefore, typical variations in T and M_w as given in Table 2 will have a larger impact on the total cost (J_T) than Z and $P_{z,0}$ due to model-plant mismatch or controller tuning.

6. Industrial Case Study

This section discusses the implementation of a pressure buffering control scheme on an industrial gas header. The industrial process is described in Section 6.1, the gain multiplication calculations are discussed in Section 6.2, and the case

study results are presented in Section 6.3. The CLMPC method is selected as the buffering control scheme for the case-study due to the following considerations:

- The CLMPC scheme performed well in Section 5.1.
- Turn-key MPC solutions are less invasive than regulatory changes on the base-layer control level for testing purposes.
- The CLMPC scheme can easily be implemented using commercial MPC applications.
- It is impractical to build a large number of control schemes on an industrial plant for comparison and find operating regions where the process is such that all other influences are negligible. Therefore, only the existing control strategy (PI) and a selected buffering control strategy (CLMPC) is built on the real process.

6.1. Process Description

Fig. 9 shows a high level diagram of the industrial case study. There are two headers which connect a supplier to a consumer and are separated by parallel compressors which are treated as a single compressor using a total flow controller as illustrated in Fig. 3. Header 1 receives gas from two uncontrolled suppliers (Q_1 and Q_3) and gas can be flared at the header inlet during high pressure scenarios through a manipulated flow (Q_2). The flow through the compressors (Q_4) can be manipulated and pulls low pressure gas from Header 1 and supplies high pressure gas to Header 2. High pressure gas can be flared at the inlet of Header 2 through a manipulated flow (Q_5) and supplies two consumers. One uncontrolled consumer pulls gas from the inlet of Header 2 (Q_6). The other consumer on Header 2 can be manipulated (Q_7) at the outlet of Header 2. Header 1 uses the outlet header pressure ($P_{L,1}$) and Header 2 uses the inlet header pressure ($P_{z,2}$) as the chosen pressure measurement for control purposes. It should be noted that the following steady state mass balances hold for the pressure nodes in Fig 9:

$$Q_{z,1} = Q_1 - Q_2, \tag{49a}$$
$$Q_{L,1} = Q_4 - Q_3, \tag{49b}$$
$$Q_{z,2} = Q_4 - Q_5 - Q_6, \tag{49c}$$
$$Q_{L,2} = Q_7. \tag{49d}$$

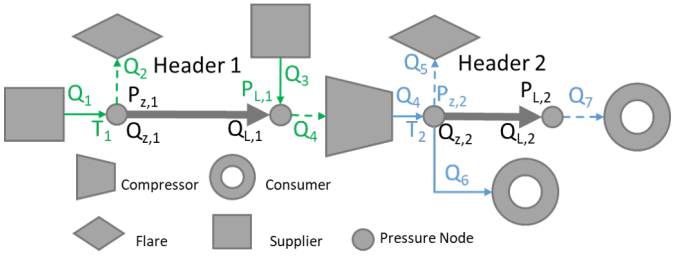

Figure 9: Industrial case study process diagram. Dashed lines indicate variables which may be manipulated. Header 1 and Header 2 are on separate redundant DCSs as indicated by the green and blue highlighted text.

Header 1 and Header 2 are on separate redundant DCSs as indicated by the green and blue highlighted text in Fig. 9 respectively. It should be noted that Q_4 is a MV for Header 1 but a DV for Header 2. The existing individual base-layer header manipulated flows and flares are combined using a deviation control MISO strategy as shown in Fig. 4. There are a number of case study specific considerations:

- There is a negligible difference in product and compression cost between flaring low pressure or high pressure gas at Q_2 and Q_5 respectively.
- Q_3 and Q_6 are never in use at the same time. Q_6 was in use during the test. Therefore, only the composition of Q_1 has influence on the molecular weight (M_w) of Header 1 and Header 2 for the duration of the test.
- Header 1 has an allowable pressure range of 40 kPa and Header 2 has an allowable pressure range of 14 kPa. Both headers are assumed to have a constant diameter of $0.944m$. The header lengths are fitting parameters [38] with values of $2683m$ and $1258m$ for Header 1 and Header 2 respectively. Header 1 has more volume and allowable pressure deviation than Header 2. Therefore, Header 1 has more buffering capacity than Header 2.
- Short pipes (< 100m) at the header inlets and outlets are combined into a single pressure node [38].

6.2. Gain Multiplier Calculation

The gain multiplier is calculated using (47) for Header 1 and Header 2. The molecular weight input is the same for both headers. The temperatures are measured at the header inlets and are assumed constant throughout the header as the pipelines are well insulated. The compressibility factors are assumed to be constant for the gain multiplier calculation as the compressibility factor has a small impact on the final cost as shown in Section 5.2. The compressibility factor values are chosen as 0.95 for Header 1 and 0.97 for Header 2 respectively.

Fig. 10 shows the calculated gain multipliers ($K_{p,1}$ and $K_{p,2}$) over a period of 16 days for Header 1 and Header 2 respectively. From the daily variations in $K_{p,1}$ and $K_{p,2}$ it can be seen that temperature changes in T_1 and T_2 contribute up to 2% deviations in the gain multipliers due to day-night ambient temperature variations. From the weekly large variations in $K_{p,1}$ and $K_{p,2}$ it can be seen that the molecular weight changes contribute up to 10% variations in the gain multiplier. The molecular weight variations are due to factory planning and operating region variations.

6.3. Case Study Results

The case study makes use of licensed robust model predictive control technology (RMPCT) [46], a Honeywell product, to execute the compensated linear model derived using (46). Custom VBScript code is subsequently used to calculate the gain multiplier using (47) and interfaced with the pressure CV gain multiplier through an open platform communications (OPC) interface. For commercial reasons the specific gains, weights and

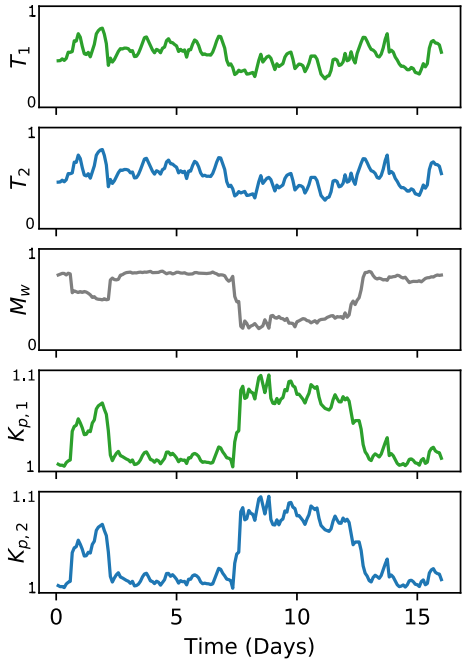

Figure 10: Gain multiplier calculation over a period of 16 days. The temperatures and molecular weight values are scaled according to the ranges shown in Table 2. $K_{p,1}$ and $K_{p,2}$ are not scaled.

tuning parameters used in the industrial Honeywell RMPCT controller are not shown.

Fig. 11 shows a comparison between time periods when the headers were controlled with a PI pressure controller tuned using standard IMC tuning rules (20) and when a buffering control scheme using the CLMPC method was used to control the header pressures. For the test period, the PI controller was active from 0 to 100 minutes and the CLMPC scheme was active from 100 to 200 minutes.

The CLMPC scheme uses the same interface point as the PI controller. Therefore, the cascaded base-layer and process setup remains the same irrespective of which controller is moving the pressure output to the flow controllers. The gain multipliers remain constant for the time duration of the test period and have values of $K_{p,1} = 1.02$ and $K_{p,2} = 1.01$. An operating time period for the test was chosen where the external influences could be considered as negligible for the two controllers.

Table 5 provides the cost of consumer stability and flaring before and after the CLMPC is turned on. It can be seen from Fig. 11 and Table 5 that the CLMPC outperforms the PI controller in terms of flow stability on Header 1 ($J_{V,1}$) and Header 2 ($J_{V,2}$), and flaring reduction on Header 2 ($J_{F,2}$). Both controllers manage to avoid flaring on Header 1 ($J_{F,1}$).

The cost of consumer stability in Q_4 ($J_{V,1}$) and Q_7 ($J_{V,2}$) is 1.3 times and 7.9 times larger when using the PI controller instead of the CLMPC buffering controller respectively. The cost of flaring at Q_5 ($J_{F,2}$) is 5.2 times larger when using the PI controller instead of the CLMPC buffering controller. The CLMPC buffering controller reduces the total cost (J_T) by a factor of 4.3 compared to the PI controller. Additionally, the improvement in Header 1 assists Header 2 as Header 1 supplies Header 2 through Q_4. These results show that using a buffering control scheme may greatly improve consumer stability and reduce flaring in industrial gas processing facilities.

Table 5: Cost of flaring and consumer stability results.

Parameter	PI	CLMPC	PI/CLMPC
$J_{V,1}$	0.76	0.57	1.3
$J_{V,2}$	0.57	0.073	7.9
$J_{F,1}$	0.0	0.0	-
$J_{F,2}$	8.4	1.6	5.2
J_T	9.7	2.3	4.3

For commercial reasons, the results reported in this section are scaled. Table 6 shows the values used to scale the inputs and outputs in Fig. 10 and Fig. 11 respectively to be between 0 and 1 relative to their operating ranges. Therefore, as an example, if the operating range of the temperatures is $295K$ to $330K$, $295K$ is scaled to 0 and $330K$ is scaled to 1. $K_{p,1}$ and $K_{p,2}$ are ratios and are not scaled.

Table 6: Scaling ranges used for the industrial case study.

Parameter	Range	Units
Temperatures	35	K
Molecular Weight	3	kg/kmol
Pressures	60	kPa
Flows	15	kg/s

A fast Fourier transform (FFT) analysis, with results shown in Table 7, is used to determine the typical disturbance amplitudes and periods which the pressure controllers have to reject for the duration of the test period. Only the frequencies with the highest and second highest amplitudes are shown. Signals with lower amplitudes and higher frequencies are assumed to be process and measurement noise.

Table 7: FFT spectral analysis of the first two highest disturbance signals.

Flow	Amplitude (kg/s)	Period (min)
$Q_{z,1}$	1.06	50
$Q_{z,1}$	0.35	25
$Q_{z,2}$	0.96	50
$Q_{z,2}$	0.38	20

From Table 7 it can be seen that the headers have to reject slow disturbances with periods of 50 minutes, and medium disturbances with periods of 20 to 25 minutes. This is similar to the disturbances used for the simulations in Section 5.1.

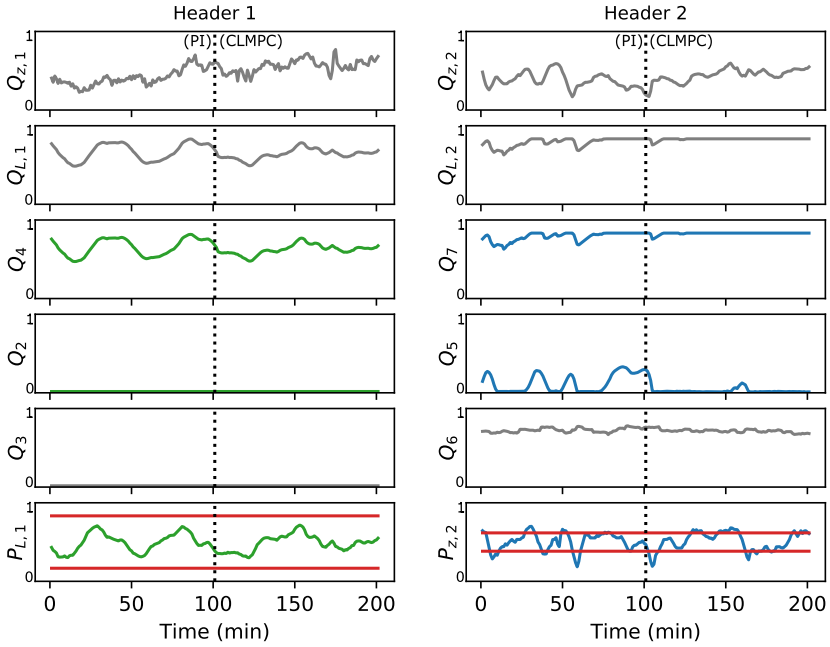

Figure 11: Industrial case study results. Vertical dashed black lines indicate when the control action was switched from PI to the CLMPC. Horizontal solid red lines indicate desired pressure limits to be used for buffering capacity.

7. Conclusion

This paper provides an overview of pressure buffering control in industrial gas headers with emphasis placed on reducing gas emissions and improving consumer stability. Various regulatory, advanced regulatory, and model predictive control schemes are evaluated based on cost functions. Averaging level control techniques are investigated and modified for pressure buffering control. The costs of flaring, consumer stability, expensive supplier use, and controller complexity are used to compare the controllers using a Monte Carlo simulation.

The sensitivity of the gas properties on the total cost were analysed using the Sobol method. It was found that given the parameter ranges in this study, the molecular weight and temperature have a large impact on the cost and that the compressibility factor and operating pressure have little impact on the total cost.

A CLMPC scheme is selected and applied on an industrial gas header system and compared with standard PI control. It was found that the CLMPC scheme is able to exploit the available buffering capacity and outperforms the PI controller in consumer stability and gas emissions substantiating the benefits of buffering pressure control.

Future work may expand buffering control to large networks of pipelines. This may include real time optimisation objectives such as power consumption and cooperative buffering between headers to meet individual consumer stability targets. A deviation MISO control strategy was used in the current study and future work may investigate the various applications of the different MISO control strategies specifically for header pressure control. The result that a higher number of NTP and NPO generally results in a lower total cost is interesting and future work may investigate if it could be related to a broader control design concept. The solutions presented in this study may be expanded to applications outside of CTL and GTL facilities.

References

[1] C. Muller, I. Craig, N. Ricker, Modelling, validation, and control of an industrial fuel gas blending system, Journal of Process Control 21 (6) (2011) 852–860.

[2] N. Ricker, C. Muller, I. Craig, Fuel-gas blending benchmark for economic performance evaluation of advanced control and state estimation, Journal of Process Control 22 (6) (2012) 968–974.

[3] A. H. Lillebø, A. Holmen, B. C. Enger, E. A. Blekkan, Fischer Tropsch conversion of biomass-derived synthesis gas to liquid fuels, Wiley Interdisciplinary Reviews: Energy and Environment 2 (5) (2013) 507–524.

[4] A. De Klerk, Fischer-Tropsch Refining, John Wiley and Sons, 2012.

[5] S. Fourie, Advanced process monitoring using wavelets and non-linear principal component analysis, Appendix D, Master's thesis, University of Pretoria (2007).

[6] J. Liu, A. Zhang, X. Jiang, M. Liu, J. Zhu, C. Song, X. Guo, Direct transformation of carbon dioxide to value-added hydrocarbons by physical mixtures of Fe5C2 and K-modified Al2O3, Industrial & Engineering Chemistry Research 57 (28) (2018) 9120–9126.

[7] H. Puliyalil, D. L. Jurković, V. D. Dasireddy, B. Likozar, A review of plasma-assisted catalytic conversion of gaseous carbon dioxide and methane into value-added platform chemicals and fuels, RSC Advances 8 (48) (2018) 27481–27508.

[8] Y. Zhang, A. H. Sahir, E. C. Tan, M. S. Talmadge, R. Davis, M. J. Biddy, L. Tao, Economic and environmental potentials for natural gas to enhance biomass-to-liquid fuels technologies, Green Chemistry 20 (23) (2018) 5358–5373.

[9] H. Atashi, S. Veiskarami, Green fuel from coal via Fischer–Tropsch process: Scenario of optimal condition of process and modelling, International Journal of Coal Science & Technology 5 (2) (2018) 230–243.

[10] E. A. Emam, Gas flaring in industry: An overview, Petroleum & Coal 57 (5) (2015).

[11] A. Mishra, S. Gautam, T. Sharma, Effect of operating parameters on coal gasification, International Journal of Coal Science & Technology 5 (2) (2018) 113–125.

[12] I. K. Muritala, D. Guban, M. Roeb, C. Sattler, High temperature production of hydrogen: Assessment of non-renewable resources technologies and emerging trends, International Journal of Hydrogen Energy (2019).
[13] A. M. Syed, Environment, social, and governance (ESG) criteria and preference of managers, Cogent Business & Management 4 (1) (2017) 1340820.
[14] D. Marqués, M. Morari, Online optimization of gas pipeline networks, Automatica 24 (4) (1988) 455–469.
[15] M. Abbaspour, P. Krishnaswami, K. S. Chapman, Transient optimization in natural gas compressor stations for linepack operation, Journal of Energy Resources Technology 129 (2007) 314–325.
[16] R. Burlacu, H. Egger, M. Groß, A. Martin, M. E. Pfetsch, L. Schewe, M. Sirvent, M. Skutella, Maximizing the storage capacity of gas networks: A global MINLP approach, Optimization and Engineering 20 (2) (2019) 543–573.
[17] G. Zhu, M. A. Henson, L. Megan, Dynamic modeling and linear model predictive conntrol of gas pipeline networks, Journal of Process Control 11 (2001) 129–148.
[18] A. Gopalakrishnan, L. T. Biegler, Economic nonlinear model predictive control for periodic optimal operation of gas pipeline networks, Computers and Chemical Engineering 52 (2013) 90–99.
[19] A. Reyes-Lúa, C. Backi, S. Skogestad, Improved PI control for a surge tank satisfying level constraints, IFAC-PapersOnLine 51 (2018) 835–840. doi:10.1016/j.ifacol.2018.06.125.
[20] M. King, Process Control: A Practical Approach, 2nd Edition, John Wiley and Sons Ltd., West Sussex, United Kingdom, 2016.
[21] H. L. Wade, Tuning level control loops, in: B. G. Liptak (Ed.), Instrument Engineers' Handbook, Volume Two: Process Control and Optimization, CRC press, 2005, Ch. 2.36, pp. 432–441.
[22] D. E. Seborg, T. F. Edgar, D. A. Mellichamp, H. Wiley, Process Dynamics and Control, 3rd Edition, 2011.
[23] T.-F. Cheung, W. L. Luyben, Liquid-level control in single tanks and cascades of tanks with proportional-only and proportional-integral feedback controllers, Industrial and Engineering Chemistry Fundamentals 18 (1) (1979) 15–21.
[24] R. Lakerveld, B. Benyahia, P. L. Heider, H. Zhang, R. D. Braatz, P. I. Barton, Averaging level control to reduce off-spec material in a continuous pharmaceutical pilot plant, Processes 1 (3) (2013) 330–348.
[25] T.-F. Cheung, W. L. Luyben, Nonlinear and nonconventional liquid level controllers, Industrial & Engineering Chemistry Fundamentals 19 (1) (1980) 93–98.
[26] K.-L. Wu, C.-C. Yu, Y.-C. Cheng, A two degree of freedom level control, Journal of Process Control 11 (3) (2001) 311–319.
[27] A. Sausen, P. S. Sausenand, M. de Campos, The error-squared controller: a proposed for computation of nonlinear gain through Lyapunov stability analysis, Acta Scientiarum. Technology 36 (3) (2014) 497–504.
[28] R. Sanchis, J. A. Pérez, J. Martín, A new approach to averaging level control, Control Engineering Practice 19 (2011) 1037–1043.
[29] P. Rosander, A. J. Isaksson, J. Löfberg, K. Forsman, Practical control of surge tanks suffering from frequent inlet flow upsets, IFAC Proceedings Volumes 45 (3) (2012) 258–263.
[30] A. J. Taylor, T. G. La Grange, Optimize surge vessel control, Hydrocarbon Processing 81 (5) (2002) 49–52.
[31] N. Ye, T. J. McAvoy, K. A. Kosanovich, M. J. Piovoso, Optimal averaging level control for the Tennessee Eastman problem, The Canadian Journal of Chemical Engineering 73 (2) (1995) 234–240.
[32] D. Sbarbaro, R. Ortega, Averaging level control: An approach based on mass balance, Journal of Process Control 17 (2007) 621–629.
[33] M. Lee, J. Shin, Constrained optimal control of liquid level loop using a conventional proportional-integral controller, Chemical Engineering Communications 196 (2009) 729–745.
[34] P. Rosander, A. Isaksson, J. Löfberg, K. Forsman, Performance analysis of robust averaging level control, in: 2012 Conference on Chemical Process Control, Savannah, GA, USA, 11-13 January, 2012, 2012.
[35] M. W. van der Burg, P. Djavdan, Model predictive averaging level control using disturbance prediction, IFAC Proceedings Volumes 28 (12) (1995) 219–224.
[36] P. J. Campo, M. Morari, Model predictive optimal averaging level control, AIChE Journal 35 (4) (1989) 579–591.
[37] A. J. Wiid, J. D. le Roux, I. K. Craig, Pressure measurement location selection in industrial gas headers for buffering control, Computers & Chemical Engineering 145 (2021) 107178. doi:https://doi.org/10.1016/j.compchemeng.2020.107178.
[38] A. J. Wiid, J. D. le Roux, I. K. Craig, Modelling of methane-rich gas pipeline networks for simulation and control, Journal of Process Control 92 (2020) 234 – 245.
[39] A. Reyes-Lúa, S. Skogestad, Multi-input single-output control for extending the operating range: Generalized split range control using the baton strategy, Journal of Process Control 91 (2020) 1–11.
[40] D. Krishnamoorthy, K. Fjalestad, S. Skogestad, Optimal operation of oil and gas production using simple feedback control structures, Control Engineering Practice 91 (2019) 104107.
[41] F. G. Shinskey, Process Control Systems: Application, Design, and Tuning, 4th edition, Vol. 4, McGraw-Hill New York, 1996.
[42] S. Skogestad, I. Postlethwaite, Multivariable feedback control analysis and design, 2nd Edition, Wiley, Chichester, England, 2005.
[43] P. Benner, T. Stykel, Model order reduction for differential-algebraic equations: A survey, in: Surveys in Differential-Algebraic Equations IV, Springer, 2017, pp. 107–160.
[44] S. Skogestad, Simple analytic rules for model reduction and PID controller tuning, Journal of Process Control 13 (4) (2003) 291–309.
[45] A. Saltelli, P. Annoni, I. Azzini, F. Campolongo, M. Ratto, S. Tarantola, Variance based sensitivity analysis of model output. Design and estimator for the total sensitivity index, Computer Physics Communications 181 (2) (2010) 259–270.
[46] S. J. Qin, T. A. Badgwell, A survey of industrial model predictive control technology, Control Engineering Practice 11 (7) (2003) 733–764.

Appendix A. Linear and Simplified Pressure Models

Appendix A.1. Linear Matrices, Poles, and Zeros

This section has been partly reproduced from [37] for convenience. The A, B, C, and D matrices linearised at the conditions shown in Table 1 and the corresponding poles and zeros for the system described by (43) are shown below. A brief discussion around the integrating nature of the system is also given.

The A matrix is represented as,

$$A = \left.\frac{\partial \mathbf{f}(\mathbf{x},\mathbf{u})}{\partial \mathbf{x}^T}\right|_{\mathbf{x}_0,\mathbf{u}_0} = \begin{bmatrix} A_{11} & A_{12} \\ A_{21} & A_{22} \end{bmatrix}.$$

where,

$A_{11} = O_{7\text{x}7}$,

$$A_{12} = \begin{bmatrix} -1680 & -2270 & 867 & -281 & 0 & 0 & 0 \\ 454 & 0 & -628 & 173 & 0 & 0 & 0 \\ -173 & 628 & 0 & -454 & 0 & 0 & 0 \\ 140 & -434 & 1140 & -5\text{x}10^{-7} & -1140 & 434 & -140 \\ 0 & 0 & 0 & 454 & 0 & -628 & 173 \\ 0 & 0 & 0 & -173 & 628 & 0 & -454 \\ 0 & 0 & 0 & 281 & -867 & 2270 & 1680 \end{bmatrix},$$

$$A_{21} = \begin{bmatrix} 4.7 & -6.4 & 2.4 & -0.79 & 0 & 0 & 0 \\ 1.3 & 0.012 & -1.8 & 0.49 & 0 & 0 & 0 \\ -0.49 & 1.8 & 0.011 & -1.3 & 0 & 0 & 0 \\ 0.39 & -1.2 & 3.2 & 0.012 & -3.2 & 1.2 & -0.39 \\ 0 & 0 & 0 & 1.3 & 0.013 & -1.8 & 0.49 \\ 0 & 0 & 0 & -0.49 & 1.8 & 0.016 & -1.3 \\ 0 & 0 & 0 & 0.79 & -2.4 & 6.4 & -4.7 \end{bmatrix} \text{x}10^{-4},$$

$$A_{22} = \begin{bmatrix} -0.94 & 0 & 0 & 0 & 0 & 0 & 0 \\ 0 & -0.83 & 0 & 0 & 0 & 0 & 0 \\ 0 & 0 & -0.79 & 0 & 0 & 0 & 0 \\ 0 & 0 & 0 & -0.83 & 0 & 0 & 0 \\ 0 & 0 & 0 & 0 & -0.87 & 0 & 0 \\ 0 & 0 & 0 & 0 & 0 & -0.94 & 0 \\ 0 & 0 & 0 & 0 & 0 & 0 & -0.97 \end{bmatrix}.$$

The matrices B, C, and D are,

$$B = \left.\frac{\partial \mathbf{f}(\mathbf{x},\mathbf{u})}{\partial \mathbf{u}^T}\right|_{\mathbf{x}_0,\mathbf{u}_0} = \begin{bmatrix} 3400 & 0 \\ 0 & 0 \\ 0 & 0 \\ 0 & 0 \\ 0 & 0 \\ 0 & 0 \\ 0 & -3400 \\ 0.89 & 0 \\ 0 & 0 \\ 0 & 0 \\ 0 & 0 \\ 0 & 0 \\ 0 & 0 \\ 0 & 0.89 \end{bmatrix},$$

$$C = \left.\frac{\partial \mathbf{g}(\mathbf{x},\mathbf{u})}{\partial \mathbf{x}^T}\right|_{\mathbf{x}_0,\mathbf{u}_0} = \begin{bmatrix} 1 & 0 \\ 0 & 0 \\ 0 & 0 \\ 0 & 0 \\ 0 & 0 \\ 0 & 0 \\ 0 & 1 \\ 0 & 0 \\ 0 & 0 \\ 0 & 0 \\ 0 & 0 \\ 0 & 0 \\ 0 & 0 \\ 0 & 0 \end{bmatrix}^T,$$

$$D = \left.\frac{\partial \mathbf{g}(\mathbf{x},\mathbf{u})}{\partial \mathbf{u}^T}\right|_{\mathbf{x}_0,\mathbf{u}_0} = O_{2\text{x}2} = \begin{bmatrix} 0 & 0 \\ 0 & 0 \end{bmatrix}.$$

The determinant of A is,

$$\det(A) = -9.9562\text{x}10^{-20} \approx 0.$$

A value of 0 indicates that the A matrix is singular which is further confirmed by the rank of A which is less than the amount of states ($2(nN + 1) = 14$),

$$\text{rank}(A) = 13.$$

The singularity of A shows that at least one of the eigenvalues of A is at the origin. The poles (p_G) and zeros (z_G) of (43) are,

$$p_G = \begin{bmatrix} -0.46 \pm 1.1\text{i} \\ -0.47 \pm 1.1\text{i} \\ 0^1 \\ -0.071 \\ -0.43 \pm 0.54\text{i} \\ -0.43 \pm 0.44\text{i} \\ -0.43 \pm 0.14\text{i} \\ -0.88 \\ -0.78 \end{bmatrix}, \quad z_G = \begin{bmatrix} -0.33 \pm 0.72\text{i} \\ -0.3 \pm 0.59\text{i} \\ -0.082 \\ -0.41 \pm 0.45\text{i} \\ -0.36 \pm 0.32\text{i} \\ -0.89 \\ -0.81 \\ -0.7 \end{bmatrix}.$$

There are no right-half plane (unstable) poles or right-half plane zeros which can impose restrictions on the closed loop performance. The pole at the origin is due to the integrating nature of the header pressures. The size of the matrices and the number of poles and zeros are dependant on the choice of n and N used to spatially discretise the governing equations in (5).

[1] value rounded from $1.8\text{x}10^{-16} \approx 0$.

Appendix A.2. Simplified Header Pressure Model Derivation

The derivation of (16) used for the tuning rules is derived from (5c) as,

$$\begin{aligned} PAL &= \frac{mZRT}{M_w}, \\ \implies \frac{d}{dt}\Big(PAL\Big) &= \frac{d}{dt}\Big(\frac{mZRT}{M_w}\Big), \\ \implies \frac{d}{dt}\Big(P\Big) &= \frac{ZRT}{M_wAL}\frac{d}{dt}\Big(m\Big), \\ \implies \frac{dP}{dt} &= \frac{ZRT}{M_wAL}\Big(Q_{in} - Q_{out}\Big). \end{aligned}$$

It is assumed that only the pressure (P) and the mass (m) are functions of time (t) and that Z, R, T, A and L remain constant in time relative to P and m. It is assumed that $\frac{dm}{dt} = Q_{in} - Q_{out}$.

Appendix B. Model Predictive Control Tuning Parameters

The weighting matrices used to obtain the results shown in Table 3 for the MPCs described in Section 4.4 are,

$$\begin{aligned} W_P &= [0.5\text{x}10^{-7}], \\ W_S &= [0.1], \\ W_C &= \begin{bmatrix} 0 & 0 & 0 \\ 0 & 9 & 0 \\ 0 & 0 & 0 \end{bmatrix}, \\ W_L &= \begin{bmatrix} 1.5 & 0 & 0 \\ 0 & 0 & 0 \\ 0 & 0 & 6.3 \end{bmatrix}. \end{aligned}$$

The prediction horizon ($\mathcal{N}_P$) is chosen as 5 minutes.